Collective Transport Properties of Driven Skyrmions with Random Disorder

C. Reichhardt, D. Ray, and C. J. Olson Reichhardt

Phys. Rev. Lett. **114**, 217202 — Published 27 May 2015

DOI: 10.1103/PhysRevLett.114.217202

Collective Transport Properties of Driven Skyrmions with Random Disorder

C. Reichhardt, D. Ray, and C. J. Olson Reichhardt
Theoretical Division and Center for Nonlinear Studies,
Los Alamos National Laboratory,
Los Alamos, New Mexico 87545, USA

(Dated: April 16, 2015)

We use particle-based simulations to examine the static and driven collective phases of skyrmions interacting with random quenched disorder. We show that non-dissipative effects due to the Magnus term reduce the depinning threshold and strongly affect the skyrmion motion and the nature of the dynamic phases. The quenched disorder causes the Hall angle to become drive-dependent in the moving skyrmion phase, while different flow regimes produce distinct signatures in the transport curves. For weak disorder, the skyrmions form a pinned crystal and depin elastically, while for strong disorder the system forms a pinned amorphous state that depins plastically. At high drives the skyrmions can dynamically reorder into a moving crystal, with the onset of reordering determined by the strength of the Magnus term.

PACS numbers: 75.70.Kw,75.70.Ak,75.85.+t,75.25.-j

A wide variety of systems can be effectively modeled as collectively interacting particles moving over quenched disorder, with a transition from a pinned state to a sliding state under an applied drive. Examples include driven incommensurate charge density waves [1, 2], Wigner crystals [3, 4], colloids on various types of substrates [5–7], and vortices in type-II superconductors [8–12]. In many of these systems the particle-particle interactions are repulsive, so that in the absence of disorder a hexagonal crystal of particles forms. When quenched disorder is present, the particles may retain mostly hexagonal order if the disorder is weak, while stronger disorder can cause a proliferation of topological defects creating an amorphous or glassy state [8, 9, 13]. When an external driving force F_D is applied to pinned particles, the particles begin to move above a critical drive value F_c known as the depinning threshold. For weak disorder the particles generally depin elastically and retain their original neighbors [1, 2, 5, 7, 9], but for strong disorder the depinning becomes plastic with particles continuously changing neighbors over time, forming a fluctuating liquid-like state [4–6, 9–12]. When depinning occurs from a disordered pinned state, there can be dynamic structural transitions at drives well above F_c, where the particles dynamically order into a moving anisotropic crystal or moving smectic phase [9–11, 14–20] when the strong driving reduces the effectiveness of the pinning in the drive direction [10]. Transitions from pinned to plastic and from plastic to dynamically ordered states have been observed experimentally through features in transport measures [1, 6, 9, 11], neutron scattering [14], changes in noise fluctuations [11], and direct imaging [18].

Recently a new type of system, skyrmions in chiral magnets, has been realized that can be effectively characterized as particle-like objects interacting with random disorder [21–23]. Neutron scattering experiments showed evidence for triangular skyrmion lattices in bulk MnSi samples [22], and subsequent Lorentz microscopy experiments [22–24] produced direct observations of skyrmion lattices. Imaging measurements indicate that as an externally applied magnetic field is increased, a low-density, partially-disordered skyrmion phase emerges from a helical phase before forming a denser ordered triangular lattice of skyrmions. At high fields, the skyrmion number decreases and the system enters a uniform ferromagnetic state [22, 23]. Similar to vortices in type-II superconductors, skyrmions have a particle-like nature and can be externally driven by the application of a current [25]. Experimental transport measurements show [26] that it is possible to obtain skyrmion velocity versus applied driving force curves with a finite depinning threshold. The current-driven motion of skyrmions has also been directly experimentally imaged [27, 28].

One aspect of skyrmions that makes them very distinct from other collectively driven systems in random disorder is the pronounced non-dissipative component in the equation of motion arising from the Magnus term [23, 29–31]. This term causes skyrmions to move *perpendicular* to the applied driving force, and it has been argued to be responsible for the low depinning threshold observed for skyrmions [23, 29–31]. The strength of the Magnus term is denoted by α_m while that of the damping is denoted by α_d. In superconducting vortex systems, $\alpha_m/\alpha_d \ll 1.0$ so the non-dissipative terms are very weak [8], whereas skyrmion systems typically have $\alpha_m/\alpha_d \sim 10$ to 40 so that the Magnus term dominates. This makes skyrmions a unique system in which to explore non-dissipative collective dynamics. Beyond basic science issues, skyrmions may be useful for a range of applications [32] which will require an understanding of skyrmion dynamics in the presence of disorder.

Here we utilize a recently developed particle-based model for skyrmion dynamics to study collective skyrmion behaviors in the presence of random quenched

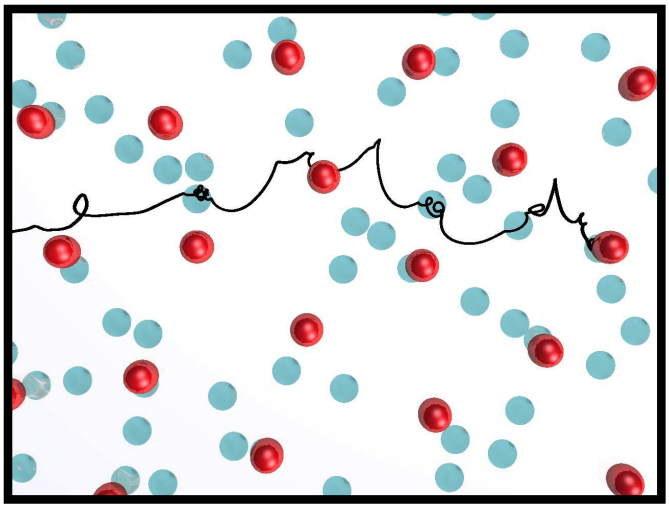

FIG. 1: Real-space image of skyrmions (dark red dots) driven through randomly arranged pinning sites (light blue dots) for a plastic flow phase at $F_p = 0.03$ and $F_D = 0.0125$. The trajectory of a single skyrmion is highlighted, showing spiraling motions inside the pinning sites.

disorder for varied disorder strengths and varied α_m/α_d. We show that the Magnus term reduces the depinning threshold and induces orbits with a circular character for skyrmions moving over pinning sites, while collective skyrmion-skyrmion interactions contribute to the reduction of the depinning threshold. We find that the Magnus term introduces a Hall angle for the skyrmion motion relative to the direction of the external drive, and that inclusion of quenched disorder strongly reduces this Hall angle, especially near depinning. At higher drives, the velocity-force curves both parallel and perpendicular to the drive show distinctive features associated with a transition into a dynamically ordered state. We also find disorder-induced transitions from a skyrmion glass to a skyrmion crystal phase as a function of disorder strength or skyrmion density.

Simulation and System— We simulate skyrmions interacting with random disorder using a recently developed particle model [31] valid for low to moderate drives in the sparse limit where the skyrmion separation and size are comparable. The dynamics of a single skyrmion i is governed by the following equation:

$$\alpha_d \mathbf{v}_i + \alpha_m \hat{z} \times \mathbf{v}_i = \mathbf{F}_i^{ss} + \mathbf{F}_i^{sp} + \mathbf{F}^D. \qquad (1)$$

Here $\mathbf{v}_i = d\mathbf{r}_i/dt$ is the skyrmion velocity. The damping term α_d aligns the skyrmion velocity with the net force acting on the skyrmion, while the Magnus term α_m rotates the velocity into the perpendicular direction. We impose the constraint $\alpha_d^2 + \alpha_m^2 = 1$ to maintain a constant magnitude of the skyrmion velocity as α_m/α_d varies. For systems such as MnSi [31], $\alpha_m/\alpha_d \approx 10$; unless otherwise noted, we take $\alpha_m/\alpha_d = 9.962$, corresponding to Magnus-dominated particle dynamics. The skyrmion-skyrmion interaction force is $\mathbf{F}_i^{ss} = \sum_{j=1}^{N_s} \hat{\mathbf{r}}_{ij} K_1(R_{ij})$ where $R_{ij} = |\mathbf{r}_i - \mathbf{r}_j|$, $\hat{\mathbf{r}}_{ij} = (\mathbf{r}_i - \mathbf{r}_j)/R_{ij}$, and K_1 is the modified Bessel function which falls off exponentially for large R_{ij}. The pinning force $\mathbf{F}_i^{sp}$ arises from randomly placed, non-overlapping harmonic traps of size $R_p = 0.3$ [31, 33] with a maximum pinning force of F_p. The driving term $\mathbf{F}^D$ represents a Lorentz force from an externally applied current interacting with the emergent magnetic flux carried by the skyrmions [26].

Our system is of size $L \times L$ with $L = 36$, has periodic boundary conditions in the x and y directions, and contains N_s skyrmions and N_p pinning sites. The pin density $\rho_p = N_p/L^2$ is fixed at 0.3, and the skyrmion density $\rho_s = N_s/L^2$ is 0.1 unless otherwise noted. We apply a slowly increasing driving force $\mathbf{F}^D$ and measure the average skyrmion velocity in the direction parallel (perpendicular) to the applied drive, $\langle V_{\rm drive} \rangle$ ($\langle V_\perp \rangle$). The Hall angle is $\theta = \tan^{-1} R$, where $R = \langle V_\perp \rangle / \langle V_{\rm drive} \rangle$. For a single skyrmion driven in the absence of disorder, $R = \alpha_m/\alpha_d$, so that $\theta = 84.25°$ in the clean limit; in contrast, a superconducting vortex with $\alpha_m/\alpha_d \approx 0.0$ would have $\theta \approx 0°$ and move in the direction of drive.

For comparison with experiment, consider an MnSi thin film [31] with lattice constant $a \approx 0.5$ nm, exchange energy $J \approx 3$ meV$/a$, and Dzyaloshinskii-Moriya energy $D \approx 0.3$ meV$/a^2$. The skyrmion size and lattice constant are $\xi \sim 2\pi J/D \approx 30$ nm, so $\rho_s = 0.1$ implies a length unit of $l_0 \approx \xi\sqrt{\rho_s} \sim 10$ nm, smaller than but comparable to ξ. The force unit is $F_0 \sim 10^{-5}$ N/m, the skyrmion-skyrmion repulsive force per length at a separation of l_0 [31]. The value $F_p = 0.03$ corresponds to a depinning force for an isolated skyrmion of $0.03F_0 = 3 \times 10^{-7}$ N/m. From the expression for the Lorentz force on a skyrmion[31], $F_L = (h/e)J$, the corresponding depinning current is $\sim 10^8$ A/m^2. Similar mappings of the simulation parameters can be performed for other materials.

Results and Discussion— In Fig. 1 we show a snapshot of skyrmions moving through random disorder in a small portion of a system with $F_p = 0.03$ and $F_D = 0.0125$. Since this drive is well above the depinning threshold $F_c \approx 0.00625$, all the skyrmions are in motion. We highlight the trajectory of a single skyrmion, which, due to the Magnus term, undergoes a circular motion within each pinning site it encounters. The force from each pinning site points toward the pin center, but under Magnus-dominated dynamics this force is largely perpendicular to the skyrmion velocity, causing the skyrmion to circle around the inner edge of the pin. In the overdamped limit $\alpha_m/\alpha_d \ll 1$, a particle entering a pinning site would quickly travel to the bottom of the potential well and be strongly pinned. We note that the escape of a skyrmion from a pin is strongly affected by motion excited via interactions with the surrounding skyrmions.

We first examine how the Hall angle is affected by random disorder. In Fig. 2(a) we plot $\langle V_{\rm drive} \rangle$ and $\langle V_\perp \rangle$ versus F_D for a system with $F_p = 0.03$. For $F_D < 0.00625$,

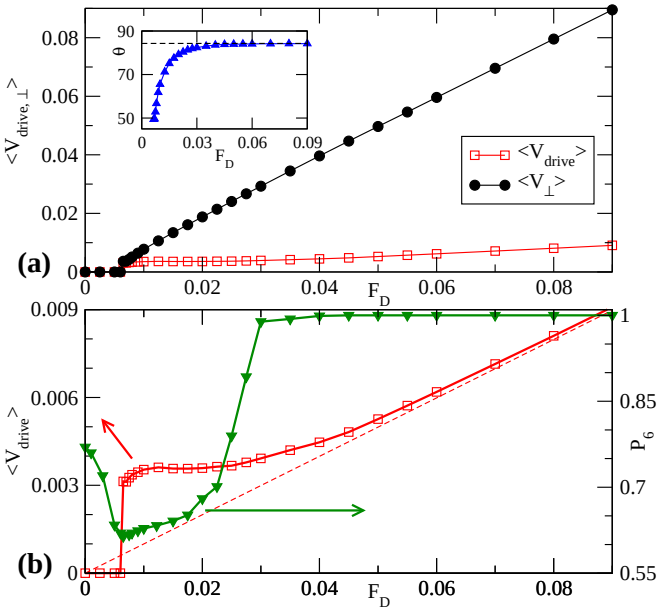

FIG. 2: (a) Average skyrmion velocity in the drive direction, $\langle V_{\rm drive}\rangle$ (open squares), and perpendicular to the drive, $\langle V_\perp\rangle$ (filled circles), vs F_D for a system with $F_p = 0.03$. Inset: Hall angle θ vs F_D; dotted line is the result for the clean system. (b) Corresponding $\langle V_{\rm drive}\rangle$ (open squares) and the fraction of sixfold coordinated particles P_6 (filled triangles) vs F_D; the dashed line shows $\langle V_{\rm drive}\rangle$ for the clean system. A dynamical ordering transition into a moving crystal state occurs at $F_D \approx 0.03$.

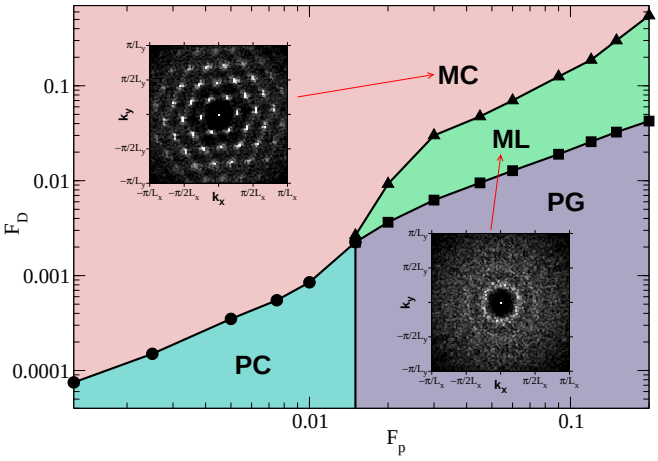

FIG. 3: Dynamical phase diagram for F_D vs F_p highlighting the different skyrmion phases. PC: pinned crystal; PG: pinned amorphous glass; ML: moving liquid; MC: moving crystal. Circles: elastic depinning from PC to MC; squares: plastic depinning from PG to ML; triangles: dynamical ordering transition from ML to MC. Upper inset: structure factor $S(\mathbf{k})$ of skyrmion positions in the MC state. Lower inset: $S(\mathbf{k})$ in the ML state.

the skyrmions are disordered and pinned. Just above depinning, $\langle V_{\rm drive}\rangle \approx \langle V_\perp\rangle$, so that $R \approx 1.0$ is much less than the clean-limit value. In general we find that adding quenched disorder decreases $\langle V_\perp\rangle$ and increases $\langle V_{\rm drive}\rangle$ compared to the clean limit, indicating that the average skyrmion flow is rotated toward the drive direction. This is illustrated in the inset of Fig. 2(a), which shows that θ falls well below the clean-limit value at low drives and approaches it at higher drives. This behavior originates from a ratcheting effect experienced by the skyrmions as they encounter pins. An applied drive displaces the equilibrium pinned position of a skyrmion from the pin center in the direction of the drive, and a skyrmion driven over a pin is pulled toward this equilibrium point. Consequently, the trajectory of a skyrmion emerging from a pin is offset in the drive direction relative to the incoming trajectory. When $F_D \lesssim F_p$, the skyrmion-pin interaction occurs for an extended time, producing a large offset, while for higher drives, the skyrmion passes quickly through the pin, diminishing the offset. Very recently, a similar dependence of the Hall angle on the drive was observed in the single-skyrmion limit [34].

As shown in Fig. 1, at $F_D = 0.0125$ the skyrmions form a disordered state; however, at higher F_D they can dynamically order into a moving crystal. In Fig. 2(b) we plot the fraction of six-fold coordinated particles P_6 as a function of F_D along with $\langle V_{\rm drive}\rangle$ for the same system as in Fig. 2(a). Readjustments of skyrmion positions in the pinned state cause P_6 to reach its smallest value at depinning where the particles are most disordered [19], but it rapidly approaches 1 around $F_D \approx 0.03$ indicating dynamical reordering. Simultaneously, $\langle V_{\rm drive}\rangle$ acquires a linear dependence on F_D and approaches the clean-limit value.

In Fig. 3 we plot a dynamical phase diagram highlighting the static and dynamic phases for skyrmions as F_D and F_p are varied. For $F_p < 0.015$ the skyrmions form a pinned triangular crystal (PC) which depins elastically to a moving crystal state (MC) as F_D increases. For $F_p > 0.015$ at low drives, we instead find an amorphous pinned skyrmion glass (PG) which depins *plastically* into a fluctuating moving skyrmion liquid (ML). The lower inset of Fig. 3 shows the structure factor $S(\mathbf{k}) = N_s^{-1}|\sum_{i=1}^{N_s} e^{-i\mathbf{k}\cdot\mathbf{r}_i}|^2$ of the ML phase, which has a liquid-like ring. As F_D increases further, the moving liquid dynamically reorders into a moving skyrmion crystal with sixfold ordering, as shown in the upper inset of Fig. 3. At $F_p \sim 0.015$ the energy scales of the skyrmion-pin and skyrmion-skyrmion interactions are equal. This phase diagram has similarities to that found for a driven vortex system [19]; however, the skyrmions reorder into a moving crystal rather than a moving smectic [35]. The vortex moving smectic forms when the pinning remains effective in the direction transverse to the drive but is weakened in the drive direction, subjecting the vortices to an anisotropic effective temperature. For moving skyrmions, additional fluctuations induced by the Magnus force reduce the transverse pinning, giving

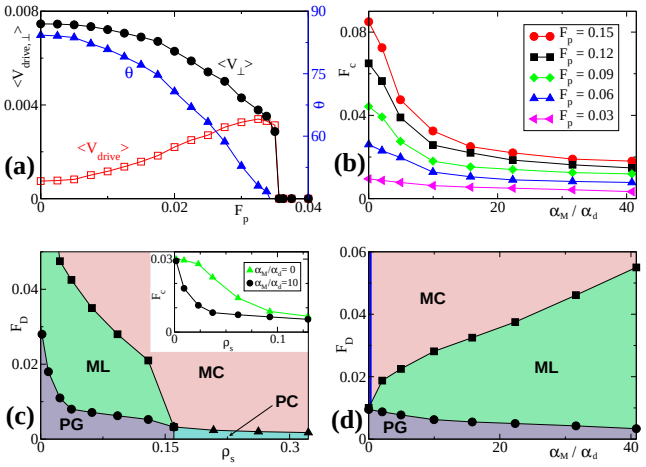

FIG. 4: (a) $\langle V_{\rm drive}\rangle$, $\langle V_\perp\rangle$, and θ vs F_p at $F_D = 0.0075$. (b) Critical depinning force F_c vs α_m/α_d for $F_p = 0.15$, 0.12, 0.09, 0.06, and 0.03 (top to bottom). (c) Phase diagram for F_D vs ρ_s at $F_p = 0.03$, highlighting the transitions from PG to ML (circles), ML to MC (squares), and PC to MC (triangles). Inset: Depinning threshold (PG-ML transition line) for Magnus-dominated (circles) and damping-dominated (triangles) systems. (d) Phase diagram of F_D vs α_m/α_d for $F_p = 0.03$, showing transitions from PG to ML (circles) and ML to MC (squares). Overdamped particles with $\alpha_m/\alpha_d = 0$ form a moving smectic state (heavy line).

a more isotropic effective temperature and allowing the skyrmions to form a more isotropic moving structure. Neutron scattering experiments could be used to observe the reordering transition from a skyrmion glass to a moving skyrmion crystal state as a function of external drive. The reordering transition is robust against changes to the pin radius [35].

To better understand how the pinning affects skyrmion motion, in Fig. 4(a) we plot $\langle V_{\rm drive}\rangle$ and $\langle V_\perp\rangle$ for fixed $F_D = 0.0075$ and varied pinning strength. As F_p increases and the skyrmions transition from MC to ML to PG (shown in Fig. 3), the trajectory offset effect caused by the pinning becomes more prominent with $\langle V_{\rm drive}\rangle$ increasing and $\langle V_\perp\rangle$ decreasing from their clean-limit values, and the Hall angle falling to a minimum of 43° at $F_p = 0.035$, near the pinning transition. In Fig. 4(b) we plot F_c versus α_m/α_d for varied F_p. As the dynamics become increasingly Magnus-dominated, F_c decreases monotonically, confirming that inclusion of Magnus forces lowers the depinning threshold. This effect is more prominent for higher values of F_p.

To show how collective skyrmion-skyrmion interactions influence the pinning, we fix F_p and vary the skyrmion density ρ_s to produce the phase diagram shown in Fig. 4(c). At low ρ_s, a disordered pinned state forms that depins plastically into a moving liquid and then orders into a moving crystal at higher drives. At higher ρ_s, a pinned crystal state elastically depins directly into a moving crystal state. The depinning threshold is very close to F_p at low ρ_s near the single skyrmion limit, but drops rapidly as ρ_s increases, indicating that *collective* skyrmion-skyrmion interactions play a crucial role in depressing the depinning threshold in a Magnus-dominated system. The inset of Fig. 4(c) shows the plastic depinning threshold for Magnus-dominated and damping-dominated particle dynamics. At low ρ_s, F_c is nearly the same for the two systems; however, as ρ_s increases and the skyrmion-skyrmion interactions become important, F_c decreases much more rapidly in the Magnus-dominated system. In Fig. 4(d) we show how the dynamical phase diagram changes as the dynamics become increasingly Magnus-dominated by plotting the phases as a function of F_D and α_m/α_d. When $\alpha_m/\alpha_d = 0$, the behavior is the same as that of a vortex system and the system reorders into a moving smectic rather than a moving crystal. As α_m/α_d increases, the depinning threshold drops while the drive at which dynamical reordering occurs increases due to the enhanced swirling motion of the skyrmions in the liquid state, which produces an effective temperature that is more isotropic and larger in magnitude than the overdamped case.

Summary— We have investigated the depinning dynamics of skyrmions interacting with random disorder, utilizing a particle-based skyrmion model. We find that the Magnus-dominated dynamics of skyrmions decreases the depinning threshold due to the swirling orbits followed by skyrmions interacting with pinning sites. Skyrmion-skyrmion scattering can excite such orbits and also plays an important role in reducing the depinning threshold. For increasing disorder strength we find transitions from a pinned skyrmion crystal to an amorphous skyrmion glass. We also show that the Hall angle deviates from its clean-limit value for strong pinning or weak driving. At high drives, unlike superconducting vortices which dynamically reorder into a smectic state, the skyrmions undergo a dynamical phase transition from a fluctuating driven liquid to a moving crystal since the Magnus term tends to make the fluctuations, and the resulting effective temperature, experienced by the skyrmions more isotropic than in a driven damping-dominated system. Features in the transport response such as velocity-force curves or structure factor measurements can be used to identify the different dynamical phases.

We thank S.-Z. Lin for useful discussions. We gratefully acknowledge the support of the U.S. Department of Energy through the LANL/LDRD program for this work. This work was carried out under the auspices of the NNSA of the U.S. DoE at LANL under Contract No. DE-AC52-06NA25396 and through the LANL/LDRD program.

[1] G. Grüner, Rev. Mod. Phys. **60**, 1129 (1988).
[2] L. Balents and M.P.A. Fisher, Phys. Rev. Lett. **75**, 4270 (1995).
[3] F.I.B. Williams *et al.*, Phys. Rev. Lett. **66**, 3285 (1991).
[4] M.-C. Cha and H.A. Fertig, Phys. Rev. B **50**, 14368 (1994).
[5] C. Reichhardt and C. J. Olson, Phys. Rev. Lett. **89**, 078301 (2002).
[6] A. Pertsinidis and X.S. Ling, Phys. Rev. Lett. **100**, 028303 (2008).
[7] T. Bohlein, J. Mikhael, and C. Bechinger, Nature Mater. **11**, 126 (2012).
[8] G. Blatter, M.V. Feigelman, V.B. Geshkenbein, A.I. Larkin, and V.M. Vinokur, Rev. Mod. Phys. **66**, 1125 (1994).
[9] S. Bhattacharya and M.J. Higgins, Phys. Rev. Lett. **70**, 2617 (1993).
[10] A.E. Koshelev and V.M. Vinokur, Phys. Rev. Lett. **73**, 3580 (1994).
[11] A.C. Marley, M.J. Higgins, and S. Bhattacharya, Phys. Rev. Lett. **74**, 3029 (1995).
[12] Y. Fily, E. Olive, N. Di Scala, and J.C. Soret, Phys. Rev. B **82**, 134519 (2010).
[13] M.-C. Cha and H.A. Fertig, Phys. Rev. Lett. **74**, 4867 (1995).
[14] U. Yaron *et al.*, Nature (London) **376**, 753 (1995).
[15] K. Moon, R.T. Scalettar, and G.T. Zimányi, Phys. Rev. Lett. **77**, 2778 (1996).
[16] T. Giamarchi and P. Le Doussal, Phys. Rev. Lett. **76**, 3408 (1996); P. Le Doussal and T. Giamarchi, Phys. Rev. B **57**, 11356 (1998).
[17] L. Balents, M.C. Marchetti, and L. Radzihovsky, Phys. Rev. B **57**, 7705 (1998).
[18] F. Pardo, F. de la Cruz, P.L. Gammel, E. Bucher, and D.J. Bishop, Nature (London) **396**, 348 (1998).
[19] C.J. Olson, C. Reichhardt, and F. Nori, Phys. Rev. Lett. **81**, 3757 (1998).
[20] H. Fangohr, S.J. Cox, and P.A.J. de Groot, Phys. Rev. B **64**, 064505 (2001).
[21] S. Mühlbauer, B. Binz, F. Jonietz, C. Pfleiderer, A. Rosch, A. Neubauer, R. Georgii, and P. Böni, Science **323**, 915 (2009).
[22] X.Z. Yu, Y. Onose, N. Kanazawa, J.H. Park, J.H. Han, Y. Matsui, N. Nagaosa, and Y. Tokura, Nature (London) **465**, 901 (2010).
[23] N. Nagaosa and Y. Tokura, Nature Nanotechnol. **8**, 899 (2013).
[24] X.Z. Yu, N. Kanazawa, Y. Onose, K. Kimoto, W.Z. Zhang, S. Ishiwata, Y. Matsui, and Y. Tokura, Nature Mater. **10**, 106 (2011).
[25] F. Jonietz, S. Mühlbauer, C. Pfleiderer, A. Neubauer, W. Münzer, A. Bauer, T. Adams, R. Georgii, P. Böni, R.A. Duine, K. Everschor, M. Garst, and A. Rosch, Science **330**, 1648 (2010).
[26] T. Schulz, R. Ritz, A. Bauer, M. Halder, M. Wagner, C. Franz, C. Pfleiderer, K. Everschor, M. Garst, and A. Rosch, Nature Phys. **8**, 301 (2012).
[27] X.Z. Yu, N. Kanazawa, W.Z. Zhang, T. Nagai, T. Hara, K. Kimoto, Y. Matsui, Y. Onose, and Y. Tokura, Nature Commun. **3**, 988 (2012).
[28] X.Z. Yu, Y. Tokunaga, Y. Kaneko, W.Z. Zhang, K. Kimoto, Y. Matsui, Y. Taguchi, and Y. Tokura, Nature Commun. **5**, 3198 (2014).
[29] J. Iwasaki, M. Mochizuki, and N. Nagaosa, Nature Commun. **4**, 1463 (2013).
[30] J. Iwasaki, M. Mochizuki, and N. Nagaosa, Nature Nanotechnol. **8**, 742 (2013).
[31] S.-Z. Lin, C. Reichhardt, C.D. Batista, and A. Saxena, Phys. Rev. B **87**, 214419 (2013).
[32] A. Fert, V. Cros, and J. Sampaio, Nature Nanotechnol. **8**, 152 (2013).
[33] Ye-Hua Liu and You-Quan Li, J. Phys.: Condens. Matter **25**, 076005 (2013).
[34] J. Müller and A. Rosch, Phys. Rev. B **91**, 054410 (2015).
[35] Movies and R_p vs F_d phase diagram available in EPAPS supplemental material.